2002–2582

ACOUSTIC SOURCE TERMS FOR THE LINEAR EULER EQUATIONS ON CONSERVATIVE FORM

Mattias Billson*, Lars-Erik Eriksson*† and Lars Davidson*
* *Department of Thermo and Fluid Dynamics, Chalmers University of Technology, SE-412 96 Göteborg, Sweden*
† *Volvo Aero Corporation, Military Engines Division, SE-461 81 Trollhättan, Sweden*

A rather novel approach to predict jet noise is the Stochastic Noise Generation and Radiation (SNGR) method. The SNGR method uses the linear Euler equations as an acoustic analogy together with source terms which are modeled. In other studies (Bechara[1] and Bailly[2]) the Euler equations on primitive form are used. In the present work the linear Euler equations on conservative form are used. Due to this, new source terms have to be derived for the conservative set of equations. A formal derivation of the correct source terms for the linear Euler equations on conservative form is presented. Simplified versions of the derived source terms are also developed. To validate the derived source terms a direct simulation of a forced 2D mixing layer is carried out. The solutions to the linearized Euler equations with source terms are compared to the solution of the direct simulation and show a good agreement. All simulations are performed using Tam and Webb's[3] fourth order DRP scheme and a four step fourth order Runge-Kutta time marching technique. Artificial selective damping introduced through the numerical scheme is used to avoid spurious waves. Absorbing boundary conditions based on characteristic variables, Engquist and Majda,[4,5] are used at the free boundaries and a buffer layer is added at the outflow.

Introduction

Using a Navier Stokes solver for the near field combined with an acoustic analogy for the far field is quite common in aeroacoustics. There are a variety of analogies which could be used, Lighthill's[6] analogy for free turbulence in a homogeneous medium, Lilley's analogy,[7] Curle's[8] extension to Lighthill's analogy for the presence of solid walls just to mention a few. Lighthill's analogy is most often solved as an integral solution and limited by the assumption of sound generation and radiation in a homogeneous medium and the same holds for Curle's extension to Lighthill's analogy. Although Lilley's analogy does include refractional effects it is somewhat sensitive to the way the source terms are evaluated.[9] The linear Euler equations with source terms are not limited by the homogeneous medium assumption and can handle refractional effects and reflection at solid boundaries. The scalar wave equation governs acoustic wave propagation but not entropy and vorticity waves. The linear Euler equations on the other hand govern both acoustic propagation as well as entropy and vorticity waves.

This work is a part of the evaluation and development of the SNGR (Stochastic Noise Generation and Radiation) method originally presented by Bechara[1] and further developed by Bailly.[2] The present work focus on the formulation of source terms for the linear Euler equations. Bailly[2] use a formulation of the linear Euler equations based on $(\rho', \overline{\rho}u', \overline{\rho}v', \overline{\rho}w', p')$ as solution variables. In that formulation, the source terms only enter the momentum equations. The formulation of the linear Euler equations used in the present work is entirely based on conservative variables, $(\rho', (\rho u)', (\rho v)', (\rho w)', (\rho e_0)')$. In this formulation the source terms enter not only the momentum equations but also the energy equation. The correct formulation of the source terms for the linear Euler equations on conservative form are derived below. It is shown that the source terms not only depend on the unsteady Reynolds stresses but also on unsteady total enthalpy. This causes some problems in the SNGR method. In the present formulation of the SNGR,[2] only velocity fluctuations are modeled, assuming that all other variables are constant. For this reason different simplifications of the source terms are derived.

The use of a forced 2D mixing layer as a test case for different methods of sound prediction was first presented by Colonius.[9] Colonius performed a direct numerical simulation of a free mixing layer

forced at its first three harmonics. The results were used and compared with Lilley's acoustic analogy.[7] Later Bogey[10] made a sound prediction with LES and Lighthill's analogy on a free mixing layer excited by the first two harmonics. The results were in both cases in good agreement between the direct simulations and the analogies. To validate the derived source terms a forced mixing layer is computed by direct simulation using a 2D compressible Navier-Stokes solver. The solution from the direct simulation provides a reference solution (time average) and is used to evaluate the source terms for the linear Euler equations which are solved and the results are compared. Comparisons of the computational results using the different source terms with direct simulation of a forced free mixing layer are presented and discussed.

Theory

In this section a derivation of the linearized Euler equations and energy equation on conservative form with source terms is presented. The derivation starts with the Euler equations and is a rewriting of the full Euler equations in a way that the left hand side of the equations are the linear Euler equations. The remaining non-linear terms in this derivation are put in the right hand side and form the source terms.

Start with the compressible Euler equations on conservative form.

$$\frac{\partial \rho}{\partial t} + \frac{\partial \rho u_j}{\partial x_j} = 0 \tag{1}$$

$$\frac{\partial \rho u_i}{\partial t} + \frac{\partial}{\partial x_j}(\rho u_i u_j + p\delta_{ij}) = 0 \tag{2}$$

$$\frac{\partial \rho e_0}{\partial t} + \frac{\partial}{\partial x_j}(\rho h_0 u_j) = 0 \tag{3}$$

where $(\rho, \rho u, \rho v, \rho w, \rho e_0)$ are the density, the x, y and z momentum and total internal energy per unit volume; ρh_0 is the total enthalpy per unit volume. Introducing a decomposition of the variables in a time averaged part and a fluctuating part as

$$\begin{aligned} \rho &= \overline{\rho} + \rho' \\ u_i &= \widetilde{u}_i + u_i'' \\ p &= \overline{p} + p' \\ e_0 &= \widetilde{e}_0 + e_0'' \\ h_0 &= \widetilde{h}_0 + h_0'' \end{aligned} \tag{4}$$

where bar denotes time averaged and prime fluctuating variable. The average of for example u_i is a Favre time average defined by

$$\widetilde{u}_i = \frac{\overline{\rho u_i}}{\overline{\rho}} \tag{5}$$

and the double prime is the fluctuation associated with the Favre time averaged velocity.

The momentum can be decomposed in two ways

$$\begin{aligned} &\rho u_i = \overline{\rho u_i} + (\rho u_i)' = \overline{\rho}\widetilde{u}_i + (\rho u_i)' \quad \text{or} \\ &\rho u_i = \rho(\widetilde{u}_i + u_i'') = \rho\widetilde{u}_i + \rho u_i'' \end{aligned} \tag{6}$$

$$\Rightarrow (\rho u_i)' = \rho'\widetilde{u}_i + \rho u_i'' \tag{7}$$

The first decomposition in equation 6 is done by time averaging ρu_i and the second by Favre averaging u_i. Both are valid and will be used in the following derivation. Combined they give equation 7. The same holds for ρe_0 and ρh_0 which gives the following equalities

$$\begin{aligned} (\rho e_0)' &= \rho'\widetilde{e}_0 + \rho e_0'' \\ (\rho h_0)' &= \rho'\widetilde{h}_0 + \rho h_0'' \end{aligned} \tag{8}$$

Furthermore

$$\begin{aligned} \rho h_0 u_j &= \rho(\widetilde{h}_0 + h_0'')(\widetilde{u}_j + u_j'') \\ &= \rho\widetilde{h}_0\widetilde{u}_j + \rho\widetilde{h}_0 u_j'' + \rho h_0''\widetilde{u}_j + \rho h_0'' u_j'' \end{aligned} \tag{9}$$

$$\Rightarrow \overline{\rho h_0 u_j} = \overline{\rho}\widetilde{h}_0\widetilde{u}_j + \overline{\rho h_0'' u_j''} \tag{10}$$

Taking the time average of the continuity equation 1 gives

$$\frac{\partial \overline{\rho}}{\partial t} + \frac{\partial \overline{\rho u_j}}{\partial x_j} = 0 \tag{11}$$

Subtraction of equation 11 from equation 1 results in the continuity equation for the fluctuations

$$\frac{\partial \rho'}{\partial t} + \frac{\partial (\rho u_j)'}{\partial x_j} = 0 \tag{12}$$

Averaging the inviscid momentum equation 2 gives

$$\frac{\partial \overline{\rho}\widetilde{u}_i}{\partial t} + \frac{\partial}{\partial x_j}(\overline{\rho}\widetilde{u}_i\widetilde{u}_j + \overline{\rho u_i'' u_j''} + \overline{p}\delta_{ij}) = 0 \tag{13}$$

and subtracting the resulting equation 13 from 2 gives an equation for the fluctuations

$$\begin{aligned} &\frac{\partial \rho u_i - \overline{\rho}\widetilde{u}_i}{\partial t} + \\ &\frac{\partial}{\partial x_j}(\rho u_i u_j - \overline{\rho}\widetilde{u}_i\widetilde{u}_j - \overline{\rho u_i'' u_j''} + (p - \overline{p})\delta_{ij}) = 0 \end{aligned} \tag{14}$$

Using equation 6 on the first term and expanding $\rho u_i u_j$ gives

$$\begin{aligned}&\frac{\partial(\rho u_i)'}{\partial t} + \\ &\frac{\partial}{\partial x_j}(\rho' \widetilde{u}_i \widetilde{u}_j + \rho u_i'' \widetilde{u}_j + \rho u_j'' \widetilde{u}_i + \\ &\rho u_i'' u_j'' - \overline{\rho u_i'' u_j''} + p' \delta_{ij}) = 0\end{aligned} \tag{15}$$

Using equation 7 on the second term and rewriting the resulting equation by moving all non-linear terms to the right hand side gives

$$\begin{aligned}&\frac{\partial(\rho u_i)'}{\partial t} + \\ &\frac{\partial}{\partial x_j}(\widetilde{u}_j(\rho u_i)' + \widetilde{u}_i(\rho u_j)' - \rho' \widetilde{u}_i \widetilde{u}_j + p' \delta_{ij}) = \\ &- \frac{\partial}{\partial x_j}(\rho u_i'' u_j'' - \overline{\rho u_i'' u_j''})\end{aligned} \tag{16}$$

Equation 16 is the linearized momentum equation on the left hand side with source terms on the right hand side. That the left hand side of 16 is the linearized momentum equation can be seen through differentiation of the term $\rho u_i u_j$ as

$$\begin{aligned}&\mathrm{d}(\rho u_i u_j) = \mathrm{d}\left(\frac{(\rho u_i)(\rho u_j)}{\rho}\right) \\ &= u_i \mathrm{d}(\rho u_j) + u_j \mathrm{d}(\rho u_i) - u_i u_j \mathrm{d}(\rho)\end{aligned} \tag{17}$$

Now we proceed to derive the linear equation for total energy. Averaging the inviscid energy equation (equation 3) gives

$$\frac{\partial \overline{\rho e_0}}{\partial t} + \frac{\partial}{\partial x_j}(\overline{\rho h_0 u_j}) = 0 \tag{18}$$

and subtracting equation 18 from equation 3

$$\frac{\partial(\rho e_0)'}{\partial t} + \frac{\partial}{\partial x_j}(\rho h_0 u_j - \overline{\rho h_0 u_j}) = 0 \tag{19}$$

Inserting the expressions 9 and 10 into equation 19 keeping the linear terms on the left side and moving the non-linear terms to the right hand side gives

$$\begin{aligned}&\frac{\partial(\rho e_0)'}{\partial t} + \frac{\partial}{\partial x_j}(\rho' \widetilde{h}_0 \widetilde{u}_j + \rho \widetilde{h}_0 u_j'' + \rho h_0'' \widetilde{u}_j) = \\ &- \frac{\partial}{\partial x_j}(\rho h_0'' u_j'' - \overline{\rho h_0'' u_j''})\end{aligned} \tag{20}$$

Using the decomposition 7 and 8, equation 20 can now be rewritten on the form

$$\begin{aligned}&\frac{\partial(\rho e_0)'}{\partial t} + \frac{\partial}{\partial x_j}(\widetilde{h}_0(\rho u_j)' + \widetilde{u}_j(\rho h_0)' - \rho' \widetilde{h}_0 \widetilde{u}_j) = \\ &- \frac{\partial}{\partial x_j}(\rho h_0'' u_j'' - \overline{\rho h_0'' u_j''})\end{aligned} \tag{21}$$

where the left side is the linear energy equation and the right hand side contains all non-linear terms. The resulting linear Euler equations with source terms are here summarized

$$\begin{aligned}&\frac{\partial \rho'}{\partial t} + \frac{\partial(\rho u_j)'}{\partial x_j} = 0 \\ &\frac{\partial(\rho u_i)'}{\partial t} + \\ &\frac{\partial}{\partial x_j}(\widetilde{u}_j(\rho u_i)' + \widetilde{u}_i(\rho u_j)' - \rho' \widetilde{u}_i \widetilde{u}_j + p' \delta_{ij}) = \\ &- \frac{\partial}{\partial x_j}(\rho u_i'' u_j'' - \overline{\rho u_i'' u_j''}) \\ &\frac{\partial(\rho e_0)'}{\partial t} + \\ &\frac{\partial}{\partial x_j}(\widetilde{h}_0(\rho u_j)' + \widetilde{u}_j(\rho h_0)' - \rho' \widetilde{h}_0 \widetilde{u}_j) = \\ &- \frac{\partial}{\partial x_j}(\rho h_0'' u_j'' - \overline{\rho h_0'' u_j''})\end{aligned} \tag{22}$$

The linear Euler equations above, equations 22, have been derived from the Euler equations without approximations or assumptions of the nature of the flow. The equations above are in fact still the non-linear Euler equations. But if one argue that the right hand side of equations 22 is in some way known, then the equations on the left hand side are the linear Euler equations. The right hand side could for example be given by a large eddy simulation or DNS which also provides the reference solution for the linear Euler equations. The equations 22 would then be an analogy for acoustic generation and radiation.

Unlike scalar wave operators, the linear Euler equations also supports vorticity and entropy waves. This is both an advantage and a disadvantage for the linear Euler equations as an analogy. The advantage is that entropy and vorticity waves generated by the source term are indeed governed by the linear Euler equations. The disadvantage is that this may cause instabilities. Stability analysis of the linear Euler equations show that vorticity and entropy waves can in some cases grow without bound in the presence of mean shear. The near field solution would then be dominated by this homogeneous solution instead of the forced solution which is sought for. This does not necessarily mean that the far field solution is affected by these instabilities. The instabilities will not radiate sound and contaminate the far field as long as the acoustic characteristic variables are not too strongly

coupled with the vorticity and entropy characteristic variables. There were no problems with instabilities in the simulations presented in the present work but it is important to know that control of entropy and vorticity waves may be necessary in some flows to avoid potential problems.

Approximations of source terms

One of the purposes of this work is to evaluate the effect of simplifications of the source terms in the linear Euler equations. In the SNGR only the velocities are modeled. This means that fluctuations of total enthalpy and density are not known. The first step in simplifying the source terms is to rewrite and approximate the heat source term in the energy equation. Begin by identifying

$$\rho h_0'' = \left(\frac{p}{\rho} - \widetilde{\left(\frac{p}{\rho}\right)}\right)\frac{\gamma}{(\gamma-1)} + \frac{1}{2}\rho\left(u_k u_k - \widetilde{u_k u_k}\right) \tag{23}$$

The first term can be written in terms of temperature. The first Reynolds term can be decomposed in Favre averages of velocities and the associated fluctuations. The last term can also be decomposed and rewritten in the same manner. After some algebra the following expression is obtained

$$\rho h_0'' = \rho C_p T'' + \rho\widetilde{u}_k u_k'' + \frac{1}{2}\rho\left(u_k'' u_k'' - \widetilde{u_k'' u_k''}\right) \tag{24}$$

which leads to

$$\rho h_0'' u_j'' = \rho C_p T'' u_j'' + \rho\widetilde{u}_k u_k'' u_j'' + \frac{1}{2}\rho\left(u_k'' u_k'' - \widetilde{u_k'' u_k''}\right) u_j'' \tag{25}$$

If we neglect trippel correlations of velocities we obtain

$$\rho h_0'' u_j'' = \rho C_p T'' u_j'' + \rho\widetilde{u}_k u_k'' u_j'' \tag{26}$$

and thus

$$\rho h_0'' u_j'' - \overline{\rho h_0'' u_j''} = C_p\left(\rho T'' u_j'' - \overline{\rho T'' u_j''}\right) + \widetilde{u}_k\left(\rho u_k'' u_j'' - \overline{\rho u_k'' u_j''}\right) \tag{27}$$

The following notation is introduced

$$\begin{aligned}\mathcal{T}_{ij} &= \rho u_i'' u_j'' - \overline{\rho u_i'' u_j''} \\ \mathcal{Q}_j &= C_p\left(\rho T'' u_j'' - \overline{\rho T'' u_j''}\right)\end{aligned} \tag{28}$$

Then the simplified source terms for the linear Euler equations can be written as

$$\begin{aligned}\text{Continuity} &= 0 \\ \text{Momentum} &= -\frac{\partial}{\partial x_j}\left(\mathcal{T}_{ij}\right) \\ \text{Energy} &= -\frac{\partial}{\partial x_j}\left(\mathcal{Q}_j + \widetilde{u}_i\mathcal{T}_{ij}\right)\end{aligned} \tag{29}$$

The next step in the simplification of the source terms is to neglect temperature fluctuations. The source terms are then

$$\begin{aligned}\text{Continuity} &= 0 \\ \text{Momentum} &= -\frac{\partial}{\partial x_j}\left(\mathcal{T}_{ij}\right) \\ \text{Energy} &= -\frac{\partial}{\partial x_j}\left(\widetilde{u}_i\mathcal{T}_{ij}\right)\end{aligned} \tag{30}$$

In the last step of simplifications of the source terms fluctuations of density are neglected, i.e.

$$\begin{aligned}\text{Continuity} &= 0 \\ \text{Momentum} &= -\frac{\partial}{\partial x_j}\overline{\rho}\left(u_i' u_j' - \overline{u_i' u_j'}\right) \\ \text{Energy} &= -\frac{\partial}{\partial x_j}\overline{u}_i\overline{\rho}\left(u_i' u_j' - \overline{u_i' u_j'}\right)\end{aligned} \tag{31}$$

where the primed velocities now are fluctuations associated with the ordinary time averaged velocities.

Numerical simulation and validation of theory

Numerical scheme

The code for direct simulation and the linear Euler code are based on the same numerical scheme. The convective terms are discretized with a six point stencil. The coefficients of Tam's[3] fourth order dispersion relation preserving finite difference scheme is converted to the equivalent finite volume coefficients. The diffusive terms in the direct simulation code are discretized using a compact second order scheme. A fourth order four step Runge-Kutta time marching technique is used for the time stepping. Artificial selective damping is used to prevent spurious waves from the boundaries and regions with stretching to contaminate the solution. The manner in which the artificial selective damping is introduced is described in Eriksson.[11]

Boundary Conditions

The mixing layer consists of an upper stream with a Mach number of $M_1 = 0.5$ and a lower stream with Mach number $M_2 = 0.25$. At the interface between the two streams a hyperbolic-tangent profile is used as inflow boundary profile. The inlet streamwise profile is

$$u_{in} = \frac{U_1 + U_2}{2} + \frac{U_1 - U_2}{2}\tanh\left(\frac{2y}{\delta_\omega(0)}\right) \qquad (32)$$

where U_1 and U_2 are the upper and lower velocities respectively. The initial vorticity thickness $\delta_\omega(0)$ defines the thickness of the incoming velocity profile, see figure 1. The velocity at the inflection point is defined by $U_0 = (U_1 + U_2)/2$. The spanwise velocity v_0 is set to zero at the inlet. The pressure and density are constant over the inlet and are set to normal atmospheric conditions. The Reynolds number for this flow based on the initial vorticity thickness $\delta_\omega(0)$ is $Re_\omega = \delta_\omega(0)U_0/\nu = 1.58 \times 10^5$.

The absorbing boundary conditions used are based on local analysis of characteristic variables, Engquist and Majda.[4,5] The boundary conditions handle radiation boundaries quite well as long as the outgoing waves to be absorbed are not at too high incidence angle and they are exact and non-reflecting for waves normal to the boundary. The amount of reflection from the radiation boundary is very small for these boundary conditions. The same holds for the inlet boundary. The reason for this is that the only disturbances reaching these boundaries are acoustic waves with comparably small amplitudes. At the outflow boundary, however, there are vorticity and entropy waves as well as acoustic waves convected through the boundary. The large difference in energy of the vorticity and entropy waves leaving the computational domain at the outflow compared to the acoustic waves cause a major problem. Although most of the energy in the outgoing vorticity and entropy waves is absorbed and only a small portion of the energy is reflected back into the computational domain, the reflected part comes back as acoustic waves contaminating the solution.

To aid the absorbing boundary conditions at the outflow region a buffer region is applied at the last section of the computational domain. The mesh is also stretched in the flow direction in this region to help attenuate disturbances through the artificial dissipation in the numerical scheme. This method of taking care of outgoing disturbances was successfully used by Colonius[9] and Bogey et al.[10] The term added to the governing equations is

$$\frac{\partial Q}{\partial t} = \cdots - \frac{c\sigma(x,y)}{\Delta x}(Q') \qquad (33)$$

where

$$\sigma(x,y) = \sigma_{max}\left(\frac{x - x_0}{x_{max} - x_0}\right)^2 \qquad (34)$$

Q denotes the solution vector and $\sigma_{max} = 0.1$; x_0 and x_{max} are the beginning and end of the buffer region. The disturbance Q' is in the direct simulation computed as $Q - \overline{Q}^*$. The term $\overline{Q}^*$ is a time average calculated using a low pass filter where the average from time step n is calculated from the average at time step $n-1$ and the solution at time step n as

$$\overline{Q}^*_{(n)} = \alpha\overline{Q}^*_{(n-1)} + (1-\alpha)Q_{(n)} \qquad (35)$$

where α is a number close to one (further details below).

The parabolic shape of $\sigma(x,y)$ ensures that the damping term will not cause reflections into the computational domain. The stretching of the mesh in the buffer region is also done gradually with very small amount of stretching at the beginning and more aggressive once the damping term in the buffer region is larger.

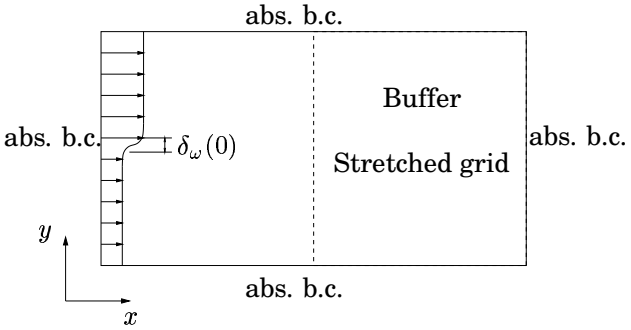

Fig. 1 Computational domain

Forcing

A two-dimensional laminar shear layer is unstable by nature and will start to break up if the computational domain is long enough. This process might take some time though and the laminar part of the shear layer can be quite long in the streamwise direction. The acoustic field produced in this process will also be more or less stochastic with peaks in the spectra for the frequencies corresponding to the natural instability frequencies of the shear layer. To get better control of the shear layer and to make it break up faster, forcing is applied at the inflow boundary. This forcing is done using the inflow absorbing boundary conditions. The incoming vorticity characteristic variable is modulated at the fundamental frequency of the incoming profile. The resulting forcing enters the spanwise inflow velocity component as

$$v_{in} = v_0 + A\sin(\omega_0 t) \qquad (36)$$

where A is the amplitude of the forcing. The forcing is only applied in the region of the hyperbolic-tangent profile. Since the forcing is included as a part of the absorbing boundary conditions, the forcing does not interfere with the absorbing property of the boundary condition and the amount of spurious waves created by the forcing is kept to

a minimum. An important detail is that the forcing added in the direct simulation is also added in the linear Euler simulation. The reasoning behind this is that unless this is done, the boundary condition for the linear Euler simulation is not consistent with the sources evaluated from the direct simulation. The result from not using forcing in the linear Euler simulation is growing instabilities.

Bogey[10] computed the fundamental frequency based on the instability theory of Michalke[12] as

$$f_0 = 0.132 \left[\frac{U_0}{\delta_\omega(0)} \right] \tag{37}$$

The shear layer is forced at two frequencies. The fundamental frequency f_0 and half the fundamental frequency $f_0/2$. In this way the forcing at the fundamental frequency will induce the creation of vortices at a frequency of f_0 which are convected downstream by the convection velocity. The second forcing at half the fundamental frequency will in turn induce a process where two successive vortices start to roll up around each other. This pair of vortices will after a short period of time start to merge and form a larger vortex. The frequency of this pairing will be denoted $f_p = f_0/2$ and the pairing time $T_p = 2T_0$. In this work, $A = 0.2$ for the forcing at the fundamental frequency f_0 and $A = 0.1$ for $f_0/2$.

Computational Setup

The computational mesh consists of 551×261 (x, y) mesh points. The physical size of the mesh is $0 \leq x \leq 6$ and $-3 \leq y \leq 3$, equivalent of $0 \leq x \leq 300\delta_\omega(0)$ and $-150\delta_\omega(0) \leq y \leq 150\delta_\omega(0)$ for $\delta_\omega(0) = 0.02[m]$. The mesh is uniform in the streamwise direction for the first 451 points with a cell length of $\Delta x = 0.375\delta_\omega(0)$. The last hundred points are used to build the buffer region in which the mesh is stretched and damping terms are added to the equations. The last cell at the outflow boundary has a cell length of $\Delta x = 4.1\delta_\omega(0)$. In the spanwise direction the mesh points are concentrated to the mixing region and stretched towards the outer boundary. The minimum cell height in the mixing region is $\Delta y = 0.164\delta_\omega(0)$ and increases slowly to $\Delta y = 0.3\delta_\omega(0)$ at $|y| \approx 5\delta_\omega(0)$. The stretching continues all the way to the boundary where the cell height is $\Delta y = 3.0\delta_\omega(0)$. With a fundamental frequency f_0 of 789Hz the emitted sound waves have a wavelength of $\lambda = 0.87[m]$ which correspond to $14\Delta y$ in the outer region so the propagating sound is well resolved in the entire domain. How the wavelength is related to the fundamental frequency will be discussed when presenting the results below.

Direct Simulation

The direct simulation started with the hyperbolic-tangent profile as initial solution. To achieve a periodic solution the simulation was run for 30 000 time steps at CFL $= 0.5$ which is equivalent to 40 pairing periods T_p. During this time the low-pass filter average (equation 35) was sampled with increasing value of the factor α. For the last 20 periods $\alpha = 0.9999$ was used before α was finally set to 1.0. This to ensure that the reference solution for the buffer layer would be representative of the true time average of the flow in the buffer layer. The sampling of the solution was then performed during 18432 time steps. With a fixed time step at CFL ≈ 0.5 this is equivalent to 24 periods with 768 time steps per period. In each time step a limited part of the solution called the source region was saved. The source region was defined as $-20\delta_\omega(0) \leq y \leq 20\delta_\omega(0)$ and $0 \leq x \leq 300\delta_\omega(0)$. The total amount of disk space required for this simulation was about 30 Gigabytes and the sampling took about 20 hours on an alpha XP-900 466 MHz processor.

Linear Euler Simulation

The linear Euler simulation used the solution from the direct simulation as initial solution and was performed during 18432 time steps. The time averaged solution from the direct simulation was used as reference solution. At each time step the solution from the direct simulation was used to evaluate the source terms. After the initial disturbances had left the computational domain the solutions could be compared. This procedure was repeated with all four sets of source terms; the full source terms (equation 22), the temperature based (equation 29), constant temperature (equation 30) and constant density source terms (equation 31).

Acoustic Solution

The far field acoustic solution is displayed by the dilatation $\partial u_i/\partial x_i$. It is favorable to use dilatation as acoustic variable instead of pressure. The pressure in the direct simulation has a tendency to fluctuate in the computation at a very low frequency. The reason for this is probably associated with the absorbing boundary conditions. This makes it hard to compare the direct simulation with the linear Euler solutions. The dilatation is in the far field related to pressure as

$$\Theta = \frac{\partial u_i}{\partial x_i} = -\frac{1}{c_0^2 \rho_0} \left(\frac{\partial p}{\partial t} + u_i \frac{\partial p}{\partial x_i} \right) \tag{38}$$

Given that the drift in pressure is linear in time the dilatation will show a non-zero but constant time average. This seems to be confirmed with the results of the dilatation of the time averaged solution which show a nearly constant and non-zero dilatation in the whole domain. The dilatation of the direct simulation is thus instead compared to the dilatation of the fluctuations of the linear Euler solutions. Vorticity is used to display the near field of the mixing layer.

Results

Figure 2 shows a snapshot of the vorticity in the near field and the dilatation in the far field for the direct simulation and the linear Euler simulation with full source terms (equation 22). The solutions seem to be very similar. The phase and amplitude also seem to be correct. Some wiggles that are visible in the direct simulation are absent in the linear solution. The reason for this is probably non-linearities in the direct simulation. The solutions from the linear Euler simulations using the simplified sources (equations 29-31) are not shown due to the fact that it is hard see any difference in the solutions compared to the full source term simulation.

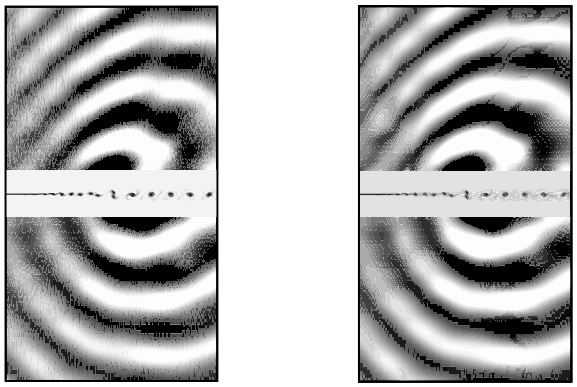

a) Direct simulation

b) Linear Euler simulation with full source terms

Fig. 2 Vorticity and dilatation for direct simulation and linear Euler equations using the full source terms, equation 22.

Figure 3 shows the instant pressure fluctuation at a line at $x = 2.0[m]$ and $0.5 \leq y \leq 3.0[m]$ for the direct simulation and the different linear Euler solutions. The average pressure has been corrected for the solution to the direct simulation to avoid the problem with the drift in the average pressure. The phase and amplitude of the linear Euler solutions are in good agreement with the direct simulation except very near the mixing layer. The deviation in this region is probably a result of the error in the time averaged pressure. The solutions for the different source terms are clearly very similar.

Figure 4 shows a pairing of two vortices at four different stages. The time difference between two subsequent figures from (a) to (d) is equivalent to one fourth of a pairing period. The pairing takes place at half the fundamental frequency so the pairing period time is $T_p = 2T_0$. During this time the merging vortices complete one half rotation around each other. The vortex pair is a rotating quadrupole and has as such four lobes. Thus, the merging process results in one full period of sound emitted at a period time of T_p, i.e. at the pairing frequency f_p of the mixing layer. The resulting wavelength of the emitted sound is $\lambda = c_0/f_p = 341.56/394.5 = 0.86[\mathrm{m}]$. It is during this time that most of the sound is generated and emitted.

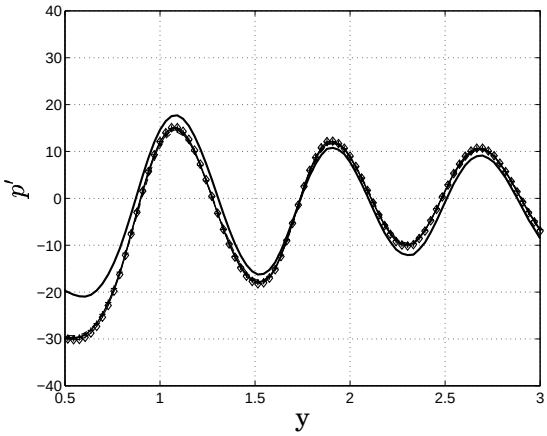

Fig. 3 Pressure disturbance at $x = 2.0[m]$, $0.5 \leq y \leq 3[m]$. Solid line: direct simulation; others: different source terms

So far the results are similar to the ones achieved by Bogey.[10] But because the physical region in this simulation is relatively a little longer than the one in Bogey,[10] there is room for merged vortices to continue emitting sound as they are convected downstream. This is evident from figure 4 where one can see that there are two regions where more sound is produced than elsewhere. This gives a slightly biased directivity with two lobes in the lower and upper regions and it is especially clear in the upper half of the computational domain.

Figure 5 shows the directivity of the time average of the square of the dilatation. Two lobes of directivity for the lower and upper regions are clearly marked at $\varphi \approx \{-95°, -54°, 39°, 76°\}$. This asymmetry in the directivity is a result of the different velocities in the upper and lower halves of the computational domain. One can again see that there are very small differences in the solutions for the different source terms.

Conclusions

The exact source terms for the linear Euler equations and the inviscid linear energy equation has been derived from the non-linear Euler equations and inviscid energy equation. Simplifications of the source terms have also been presented. These source terms have been validated through numerical simulations. The solutions from the direct simulations and the solutions from the proposed equations are in good agreement. Some differences are present but the cause is believed to be due to effects of the boundary conditions. The differences are very small between the solutions from the different source terms. Even when the source terms are based only on velocity fluctuations and all other instationary effects are neglected, the solution was nearly exactly the same as for the full source terms. This implies that the major source of sound

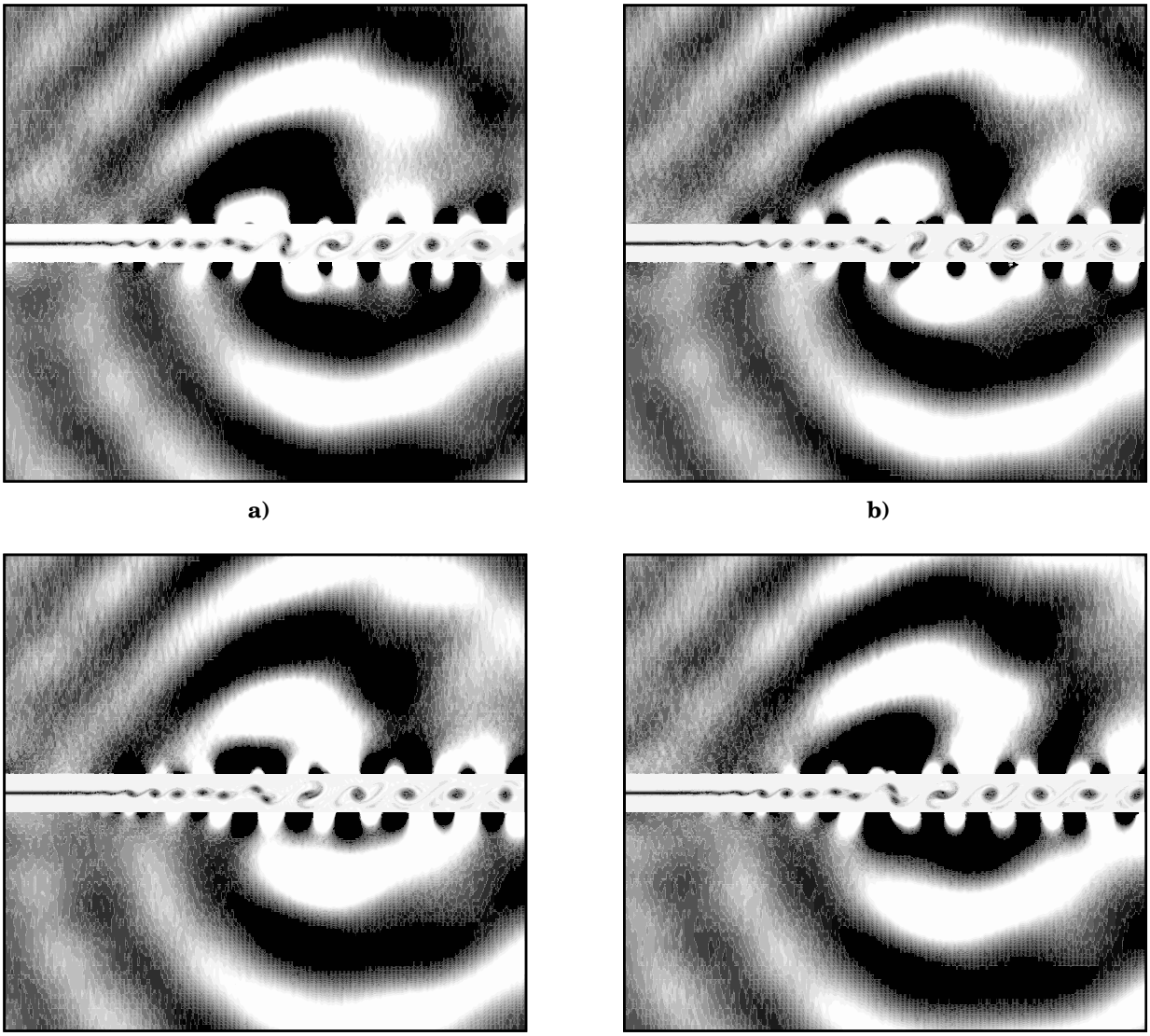

a) **b)**

c) **d)**

Fig. 4 Vorticity and dilatation for direct simulation. $0 \leq x \leq 3.26$**,** $-1.5 \leq y \leq 1.5$

in this flow is fluctuations of vorticity. Whether this is true at higher Mach numbers or with larger differences in temperature remains to be seen.

References

[1]Bechara, W., Bailly, C., and Lafon, P., "Stochastic Approach to Noise Modeling for Free Turbulent Flows," *AIAA Journal*, Vol. 32 , No. 3, 1994, pp. 455–463.

[2]Bailly, C. and Juvé, D., "A Stochastic Approach To Compute Subsonic Noise Using Linearized Euler's Equations," *AIAA Journal*, Vol. 99-1872, 1999.

[3]Tam, C. and Webb, J., "Dispersion-Relation-Preserving Finite Difference Schemes for Computational Acoustics," *J. Comp. Physics*, Vol. 107, 1993, pp. 262–281.

[4]Engquist, B. and Majda, A., "Absorbing Boundary Conditions for the Numerical Simulation of Waves," *Mathematics of Computation*, Vol. 31, 1977, pp. 629–651.

[5]Engquist, B. and Majda, A., "Radiation Boundary Conditions for Acoustic and Elastic Wave Calculations," *Communications on Pure and Applied Mathematics*, Vol. 32, 1979, pp. 313–357.

[6]Lighthill, M., "On sound generated aerodynamically, I. General theory," *Proc. Roy. Soc.*, Vol. A 211, 1952, pp. 564–587.

[7]Lilley, G., "On the noise from jets," *AGARD CP-131*, 1974.

[8]Curle, J., "The influence of solid boundaries upon aerodynamic sound," *Proc. Roy. Soc.*, Vol. A 231, 1955, pp. 505–514.

[9]Colonius, T., Lele, S., and Moin, P., "Sound generation in a mixing layer," *Journal of Fluid Mechanics*, Vol. 330, 1997, pp. 375 – 409.

[10]Bogey, C., Bailly, C., and Juvé, D., "Numerical Simulation of Sound Generated by Vortex Pairing in a Mixing Layer," *AIAA Journal*, Vol. 38 No. 12, 2000.

[11]Eriksson, L.-E., "Development and validation of highly modular flow solver versions in G2DFLOW and G3DFLOW," Internal report 9970-1162, Volvo Aero Corporation, Sweden, 1995.

[12]Michalke, A., "On the inviscid instability of the hyperbolic-tangent velocity profile," *Journal of Fluid Mechanics*, Vol. vol 19, 1964.

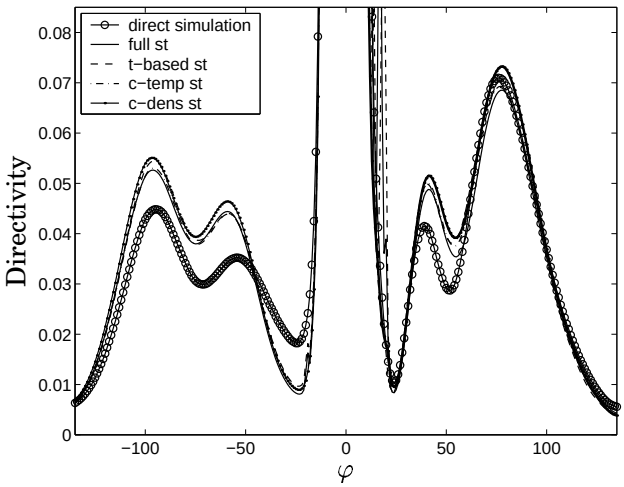

Fig. 5 Directivity displayed as time average of square of dilatation at an arc around $x_0 = 2.0$, $y_0 = 0$ with radius $r = 1.0$ at angles $-135 \leq \varphi \leq 0$ degrees from the x-axis and $x_0 = 1.6$, $y_0 = 0$ with radius $r = 1.0$ at angles $0 \leq \varphi \leq 135$ degrees. Direct simulation, full source terms (full st); temperature based (t-based st); constant temperature (c-temp st); constant density (c-dens st).